ELSEVIER

Nuclear Instruments and Methods in Physics Research A 437 (1999) 212–221

NUCLEAR INSTRUMENTS & METHODS IN PHYSICS RESEARCH Section A

www.elsevier.nl/locate/nima

A high resolution, low power time-of-flight system for the space experiment AMS

D. Alvisi[a], F. Anselmo[a], L. Baldini[a], G. Bari[a], M. Basile[a], L. Bellagamba[a], A. Bruni[a], G. Bruni[a], D. Boscherini[a], D. Casadei[a], G. Cara Romeo[a], G. Castellini[b], L. Cifarelli[a], F. Cindolo[a], A. Contin[a,*], S. De Pasquale[a], P. Giusti[a], G. Iacobucci[a], G. Laurenti[a], G. Levi[a], A. Margotti[a], T. Massam[a], R. Nania[a], F. Palmonari[a], A. Polini[a], S. Recupero[a], G. Sartorelli[a], C. Williams[a], A. Zichichi[a]

[a] *University of Bologna and INFN, Bologna, Italy*
[b] *CNR-IROE, Florence, Italy*

Received 27 April 1999; accepted 11 May 1999

Abstract

The system of plastic scintillator counters for the AMS experiment is described. The main characteristics of the detector are: (a) large sensitive area (four 1.6 m^2 planes) with small dead space; (b) low-power consumption (150 W for the power and the read-out electronics of 336 PMs); (c) 120 ps time resolution. © 1999 Elsevier Science B.V. All rights reserved.

Keywords: AMS experiment; Plastic scintillator; TOF

1. Introduction

The Alpha Magnet Spectrometer (AMS) [1] is the first large acceptance (0.65 m^2 sr) particle detector designed to operate in the space to measure, for many years, cosmic-ray fluxes. It will be installed, as part of the scientific program, on the International Space Station Alpha soon to be built, through an international co-operation effort, in a low (about 400 km) orbit around the Earth.

The AMS experiment will address two fundamental questions in astroparticle physics: the possible presence of cosmological antimatter in the universe and the nature of the so-called "dark matter". These physics goals require the measurement of particle momentum, velocity and charge with the highest possible degree of confidence and extremely accurate particle identification.

The detector configuration, shown in Fig. 1, consists of a permanent magnet equipped with six layers of high-precision silicon tracker, a time-of-flight (TOF) scintillator system, a scintillator system for the rejection of events due to interactions on the magnets inner wall and a threshold Aerogel Cherenkov system. It has been placed aboard the Space Shuttle Discovery as a precursor for a 10-day test-flight carried out in June 1998.

The TOF system is based on our previous experience and well-established techniques [2–5] able to

* Corresponding author.

0168-9002/99/$ - see front matter
PII: S0168-9002(99)00523-9

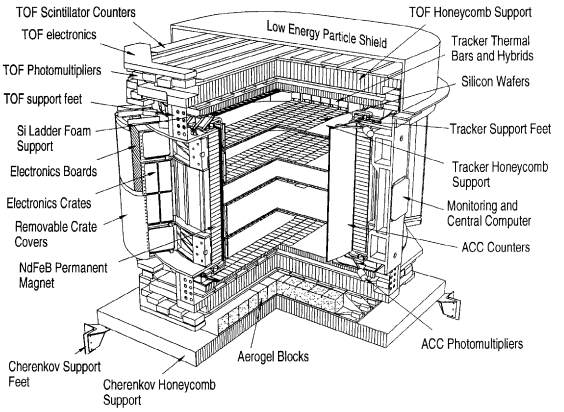

Fig. 1. The AMS detector.

reach a precision in the time resolution of 100 ps. It has been completely designed and built at the INFN Laboratories in Bologna, and it will provide:

(a) the fast trigger to the experiment,
(b) the measurement of the TOF of the particles traversing the detector with a resolution sufficient to distinguish the upward going particles from the downward going ones at a level of at least 10^{-8}–10^{-9}, and electrons from anti-protons up to about 2 GeV,
(c) the measurement of the absolute charge of the particle in addition to the measurement done by the silicon tracker.

2. Design considerations

The main parameters taken into account while designing the detector are:

(a) *Total sensitive area*: To match the full acceptance of the magnet, each plane of the TOF system has to cover a circular area of about 1.6 m^2. This has been obtained with 11 cm wide scintillator pads of different length, overlapped by 0.5 cm to avoid geometrical inefficiencies.

(b) *Trigger selection*: The TOF system has to provide the fast trigger to the AMS experiment. For an efficient background rejection, the system consists of two pairs of planes, one before and one after the magnet, with the paddles arranged perpendicularly to each other in the two planes of each pair. This allows for a granularity of about 11×11 cm^2 for trigger purposes.

(c) *Weight*: Given the strong limitations in the total weight of the AMS detector, the TOF system was allotted only about 250 kg to accommodate for the detector itself, the support structure and the power supply system.

(d) *Power consumption*: The TOF system was allowed to use about 150 W for PMs operation and signal read-out (see Section 3.2), out of the 1 kW electric power given by NASA to the AMS experiment on the Shuttle test flight.

(e) *Time-of-flight resolution*: The resolution in the TOF needed to satisfy the physics requirements outlined in Section 1 is about 100 ps. The choice made to use 1 cm thick scintillator (see Section 3), was a compromise between the minimum thickness and the light output needed to reach this resolution.

(f) *Operation in space*: The operation of the TOF system in space imposes several requirements on the mechanical design and on the servicing electronics of the TOF system. In particular, each module has to be housed in a mechanically robust and light-tight cover with a system for fast depressurization (see Section 3), the support structure has to conform to the NASA specifications concerning resistance to load and vibrations [6] and the electronics has to be protected from the highly ionized low-orbit environment (see Section 3.1). Moreover, the system has to guarantee redundancy, hence the choice of having three PMs on each side of the counters.

3. Description of the basic module and of the associated electronics

Each TOF plane is assembled out of 14 modules, overlapped by 0.5 cm. One module, shown in Fig. 2, is a 1 cm thick, 11 cm wide, 72–136 cm long BC408 scintillator paddle (index of refraction $n = 1.59$). On each side, a 5 cm long trapezoidal guide collects the scintillator light on the photocathodes of three R5900 HAMAMATSU photomultipliers, through 1.8×1.8 cm^2 cross section and 2.4 cm long straight guides. The bi-alkali photocathode sensitivity matches the scintillator light spectrum.

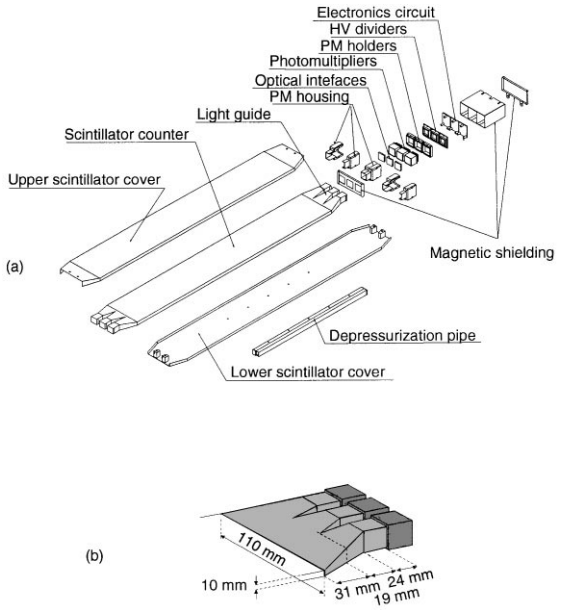

Fig. 2. (a) Exploded view of one TOF module assembly; (b) design of the light guide.

Each scintillator plate is wrapped with an aluminized mylar and put into a two-shell, 0.6 mm thick, carbon fiber cover. The PMs are fixed with a plastic housing to the light guides. In order to mechanically decouple the PMs and the scintillator paddle, a $25 \times 25 \times 3\,\mathrm{mm}^3$ optical silicon (Dow Corning 93–500) rubber sheet is used as optical contact between the light guide and the PM photocathode window.

The signals from the three PMs on each side of the scintillator paddle are summed up to provide one signal from the anodes and one from the second last dynodes. The HV distribution resistor chain is mounted on to two PCBs behind each PM. In the PCB attached to the central PM there are also the summing circuit and the cables carrying the signals out. Although the PMs can withstand a magnetic field of some Gauss without degradation in the performances, the PMs and the electronics circuits are protected from the residual magnetic field of the AMS magnet (about 200 G) by a 0.5 mm thick shielding case made of VACOFLUX permalloy.[1]

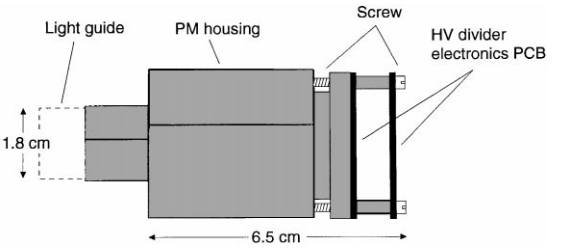

Fig. 3. Assembly of the HV dividers in the PM back.

Each module is equipped with an LED placed in the center to be used for calibration and testing purposes (see Section 5).

In addition to the HV divider and to the summing circuits already mentioned, the electronics for the HV distribution system and for the read-out and trigger have also been completely designed and built in INFN, Bologna and in CNR-IROE, Florence, Italy.

3.1. PM electronics and HV distribution system

The HAMAMATSU R5900 are small PMs ($2.4 \times 2.4 \times 2.5\,\mathrm{cm}^3$) working at -700–750 V with a gain of about 10^6, with metal casing and 10 "venetian blind" dynodes. The signal produced by a single photoelectron has a rise time of 600 ps and a time jitter of 150 ps.

The HV power supplies are based on the voltage amplifiers Bellnix MHV12-1.0k2000N[2] driven at 12 V and on electronic circuits which allows for the individual setting of each PM. Two large PCBs mounted on the top of each plane (see Fig. 1) hold two Bellnix each to produce and distribute the HV to the 42 PMs on each side. The same PCBs also distribute the trigger signal to the LEDs. The home-made control boards set the low-voltage values for each PM.

The HV dividers and the summing circuit are mounted directly on the PMs, as shown in Fig. 3. In order to avoid discharges at the operating pressure (expected to be higher than the outside pressure of 10^{-12} atm because of outgassing), and at an electric conductivity about seven orders of magnitude

[1] Vacuum Schmeltz, Germany

[2] Maximum output voltage: -1000 V; maximum current 2 mA.

larger than at ground [7], extensive tests have been carried out in a vacuum chamber at CNR-IROE. As a result, it was decided to have all the PM sockets potted with Dow Corning 93-500 silicon rubber and to coat all the exposed surfaces of the PCBs with Dow Corning 3140.

3.2. Read-out electronics

Each read-out and trigger electronics module [8] consists of a PCB holding four complete channels. Each channel provides

(a) a trigger signal (corresponding to a threshold of 150 mV on the input anode signal) which is sent to the general AMS trigger system;
(b) a high-resolution (25 ps bin size) time measurement of the delay between the input anode signal (above a threshold of 30 mV) and the trigger signal coming back from the general AMS trigger;
(c) the amplitude of the integrated input anode signal;
(d) the amplitude of the integrated input dynode signal;
(e) a time-over-threshold signal which gives a rough estimate of the signal time (with 1 ns bin size) to tag off-time events in a time interval of 10 μs before and 6.5 μs after the trigger.

From the high-resolution time measurements of the two sides of the counter (t_1 and t_2) the following quantities can be derived:

mean time: $t_m = \dfrac{t_1 + t_2}{2}$

half-time difference: $\Delta t = \dfrac{t_1 - t_2}{2}$

which can be used to compute the absolute time of passage of the particle through the counter:

$$t_0 = \frac{t_1 + t_2}{2} \tag{1}$$

and the position along the counter:

$$x = v_{\text{eff}} \frac{t_1 - t_2}{2} \tag{2}$$

where v_{eff} is the effective velocity of light in the counter.

The velocity v_{eff} can be measured if x is known from an external tracking detector (see Section 5).

The dynamic range of the anode charge measurement allows for the measurement of charge up to $|z| = 2$–$3e$. The measurement of the second dynode charge extends the dynamic range of the measurement by a factor of about 5.

4. Support structure

The individual modules are not rigid enough to resist the high accelerations and the vibrational loads induced into the experiment during the launching and landing phases of the Shuttle flight.

To provide a suitable mechanical rigidity, the modules are mounted on a support made of a 10 cm thick aluminium honeycomb panel glued between two 0.5 cm thick aluminium skins. Carbon fibre brackets are used to fix the module to the honeycomb panels. Each panel accommodates two scintillator planes.

To assure the resistance of the whole system and the capability of each module to work properly after the acceleration phase, a long procedure of design, simulation and test has been followed. This part will be described in detail in a following paper [6]. Here it is enough to say that every part of the system, from the scintillator pieces, to the PMs and the mechanical supports have been first analysed using a Finite Element Modelling (FEM) program; then a model analysis has been performed to determine the natural vibrational frequencies of the different parts, to avoid cases of natural exciting resonances.

Finally, both the initial prototype [6] and the flying modules have been successfully tested on a shaking machine following a pattern of random vibrations between 50 and 2000 Hz according to NASA specifications. This kind of test, called Acceptance Vibration Test (AVT), was performed at the Alenia Spazio–Globalstar facilities in Rome and provided a very detailed information on the dynamical behaviour of the system.

5. Performances of the modules

The development of the basic module design and the measurements of the characteristics of the counters have been done using a cosmic ray telescope in the INFN Laboratories in Bologna, with standard NIM/CAMAC trigger and readout electronics.

In addition, a complete simulation program, based on the GEANT program package and on a proprietary ray-tracing routine, has been developed to check the results from the tests and to help in optimizing the design of the module.

The cosmic ray telescope consists of two planes of limited streamer tube detectors (LST) with cathode strip read-out (1.8 cm pitch). The test counter is positioned in between the two planes, together with a reference scintillation counter of the same basic design and with known characteristics, which is used for triggering and to give a zero time to the test module. The strip direction is perpendicular to the test counter, providing the impact point position of a particle along the counter with about 5 mm precision.

5.1. Counter selection

A first set of 66 counters was built and measured using the same PMs in order to compare their light output and their time resolution. The results were used to select the best 56 counters to be used in the experiment. The relative light output of the selected counters have an r.m.s. of 4.4%, as shown in Fig. 4.

For each of the selected counters the following quantities have been measured:

(a) attenuation curve;
(b) effective velocity of light inside the counter;
(c) time resolution as a function of the position along the counter;
(d) position resolution as a function of the position along the counter;
(e) PM gain using the LEDs.

The basic methods which have been used to characterize the final modules are described in the following sections. Detailed results on one representative module illustrate the various measurements.

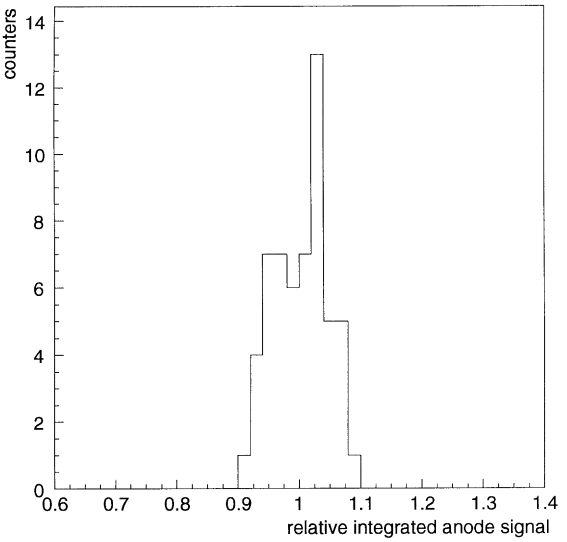

Fig. 4. Relative integrated anode signal at the center of the counters. The r.m.s. of the distribution is 4.4%.

5.2. Signal amplitude and the number of detected photoelectrons

The HV value for each PM was set so as to have equal anode signal for cosmic rays hitting the longitudinal center of the counter. A typical integrated anode signal distribution is shown in Fig. 5a.

The quantity of light seen at one side changes by about a factor of 1.5–1.6 (for a 136 cm long counter) as a function of the impact position of the particle along the counter, as shown in Fig. 5b. The data behaviour is not completely exponential as expected for bulk material,[3] due to effects like scintillator thickness, imperfections on the scintillator surface and reflections of light from the opposite side. A single-exponential fit to the attenuation curve gives an average attenuation length of about 200 cm.

The average number of photoelectrons produced in the PMs by a minimum ionizing particle hitting the center of the counter has been computed to be between 200 and 310 (depending on the length of the counter) by measuring the dispersion in the

[3] The attenuation length for bulk material quoted by the manufacturer is of 350 cm.

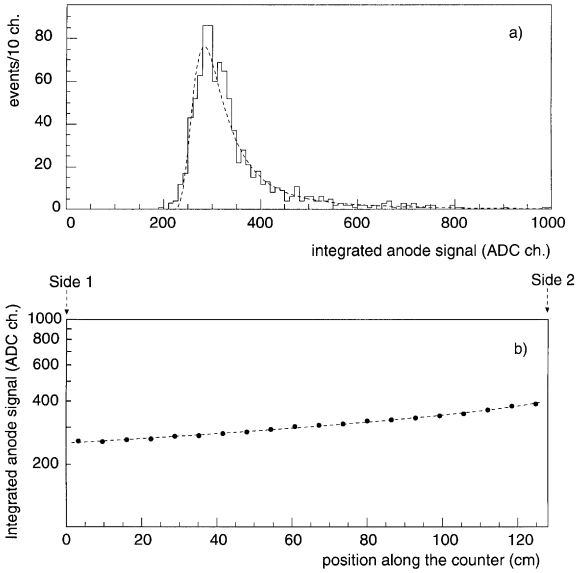

Fig. 5. (a) Integrated anode signal distribution for particles hitting the longitudinal center of the counter (1 Analog-to-Digital Converter channel = 0.25 pC). The dashed line is a fit to a Landau distribution. (b) The average integrated anode signal seen at side 2 of the counter as a function of the hit position, for a 136 cm long counter. The dashed line is a second-order polynomial fit.

signal amplitude seen at the two sides for the particles hitting the centre of the counters.

Fig. 6 shows the distribution of the ratio between the maximum and the minimum integrated anode signal seen at one side of each counter as a function of the counter length.

5.3. Slewing corrections

Time-walk (or "slewing") effects change the time of the trigger as a function of the amplitude of the signal and introduce an (asymmetric) additional term to the time resolution. Although this effect can be partially corrected for, it adds up to the intrinsic time resolution of the scintillator. Simulation studies and measurements show that the magnitude of this added resolution decreases with decreasing value of the discriminator threshold, down to a minimum of about 10% of the average signal amplitude. For practical purposes, the threshold for timing measurements ("low" threshold) was set at 30 mV. Therefore, the PMs are operated at

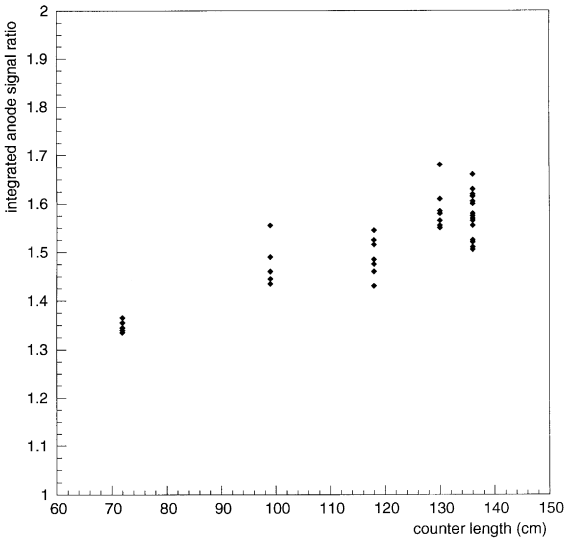

Fig. 6. The ratio between the maximum and the minimum integrated anode signal seen at one side of the counter as a function of the counter length.

a gain of about 1.2×10^6, corresponding to a signal average peak value of 300 mV for particles hitting the center of the counters.

The slewing correction formula used in the following has the form

$$t_{\mathrm{corr}} = t - \frac{k}{\sqrt{a}}$$

where t_{corr} is the corrected time, t is the measured time, a is the integrated anode signal, and k is determined by a fit to the data for each side.

The value of k is about 7.5 ns $\sqrt{\mathrm{pC}}$ for all counters.

5.4. Effective velocity of light and position resolution

The expected velocity of light in the scintillator is $v_1 = c/n = c/1.59 = 18.9$ cm/ns. Due to the difference in the path lengths of the photons which contribute to the signal at the low threshold level, the "effective" velocity of light (i.e. the distance from the PM divided by the signal timing), v_{eff}, is smaller than v_1.

Calling L the length of the counter and x the distance of the impact of the particle from side 1,

the following relation holds:

$$\Delta t = \frac{t_1 - t_2}{2} = \frac{x}{2v_{\text{eff}}} - \frac{L - x}{2v_{\text{eff}}} = \frac{x}{v_{\text{eff}}}$$

where t_1 and t_2 are corrected for the time slewing. A fit to the distribution of the average values of Δt as a function of x, measured by the cosmic ray telescope, gives the effective velocity of light in the counter.

Fig. 7 shows the distribution of the effective velocity of light for all counters.

5.5. Mean time and position resolution

The TOF between the test and the reference counter is

$$\left(\frac{t_1 + t_2}{2}\right)_{\text{ref}} - \left(\frac{t_1 + t_2}{2}\right)_{\text{test}} = \frac{d}{v_{\text{part}}}$$

where d is the particle path length and v_{part} is the particle velocity.

Assuming that the cosmic rays seen by the telescope are relativistic and that the error on the measured path length is negligible, the error on the quantity:

$$\Delta_{\text{tof}} = \left(\frac{t_1 + t_2}{2}\right)_{\text{ref}} - \left(\frac{t_1 + t_2}{2}\right)_{\text{test}} - \frac{d}{v_{\text{part}}}$$

depends only on the errors on the measured times:

$$\sigma_{\Delta_{\text{tof}}} = \frac{1}{2}\sqrt{(\sigma_{t_2}^2 + \sigma_{t_2}^2)_{\text{ref}} + (\sigma_{t_1}^2 + \sigma_{t_2}^2)_{\text{test}}}.$$

The distribution of Δ_{tof} for all particles hitting the test and reference counters is shown in Fig. 8a. A very small amount of non-Gaussian tails is

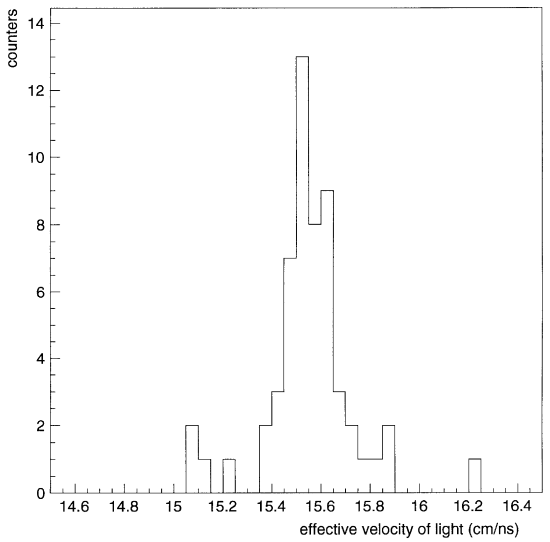

Fig. 7. Distribution of the effective velocity of light in the counters.

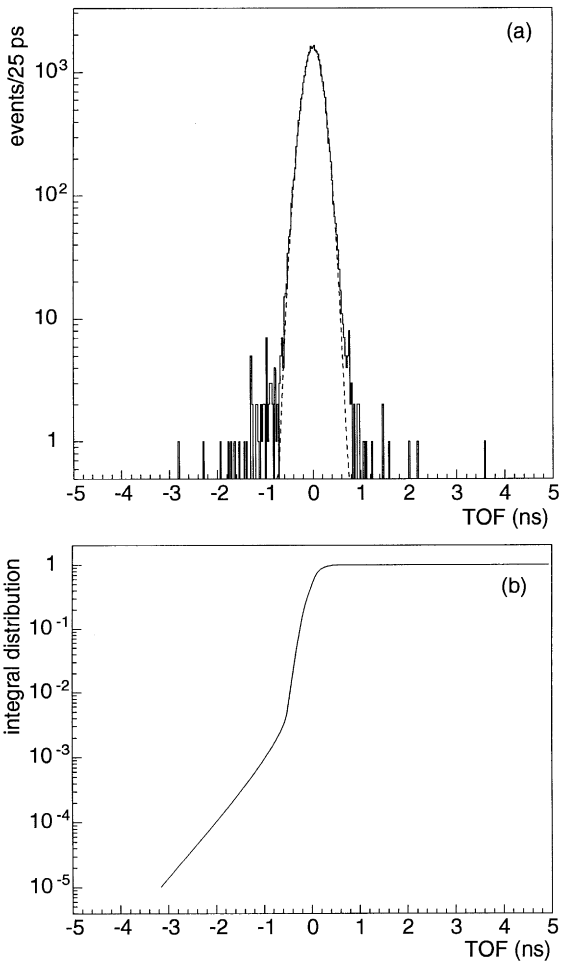

Fig. 8. (a) The TOF between the test and the reference counter corrected for the particle path length. The dashed line is a Gaussian fit with standard deviation 166 ps. (b) Integral distribution of the same quantity.

observed, most probably due to secondaries produced near to the detector.

The minimum time of flight of particles through AMS is about 5 ns. The integral distribution of Δ_{tof}, shown in Fig. 8b, indicates that the probability to misidentify the particle direction (corresponding to a value of the abscissa of -10 ns) is some order of magnitude below 10^{-5}.

In order to compute the mean-time resolution of the test counter, the mean-time resolution of the reference counter must be subtracted in quadrature. Assuming an equal resolution for the two counters, the mean-time resolution of both of them is, from Fig. 8a: $\sigma_{\Delta_{tof}}/\sqrt{2} = 117$ ps.

A more refined analysis has been done assuming that the mean-time resolution of the reference counter is the same as the resolution of its half-time difference, computed in 2 cm bins along the counter. By subtracting in quadrature this resolution from the Δ_{tof} resolution, the mean time resolution of the test counter as a function of the hit position of the particle along the counter has been derived (Fig. 9).

The time resolution of one side of the counter can be parametrized as

$$\sigma(x) = \sqrt{\frac{\sigma_1^2}{N} + \frac{\sigma_2^2 x^2}{N} + \sigma_3^2} \tag{3}$$

where σ_1 is the resolution due to the PM signal shape and to the trigger electronics, σ_2 is the resolution due to the dispersion of the photon path lengths, x is the distance from the PM, σ_3 is the electronic noise and N is the number of photoelectrons produced in the PM. From the fits of the time resolution of the two sides of the counter, $\sigma_{t_1}(x)$ and $\sigma_{t_2}(x)$ (Figs. 9a and b), the mean-time resolution can be computed as

$$\sigma_t(x) = \sqrt{\frac{\sigma_{t_1}^2(x) + \sigma_{t_2}^2(x)}{2}}. \tag{4}$$

Function (4) is superimposed to the data in Fig. 9c.

Fig. 10 shows the mean-time resolution at the center of the counters as a function of the counter length. As expected, the resolution increases with decreasing length due to the increase in the number of detected photons.

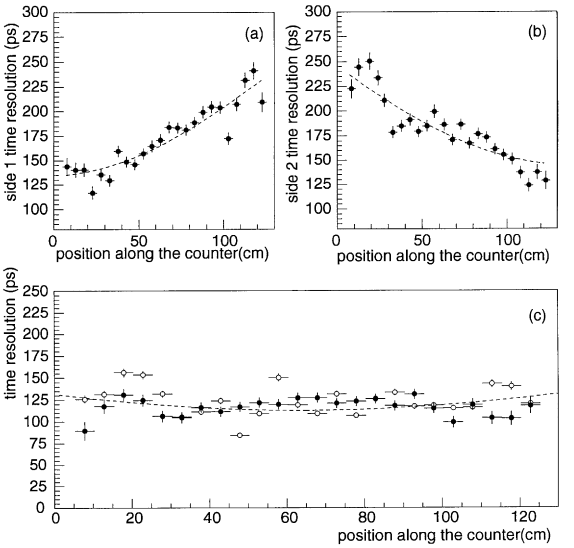

Fig. 9. The time resolution as a function of the position along the counter for a 136 cm long counter using standard NIM/CAMAC electronics. (a) Mean-time resolution of side 1. The dashed line is the fit with function (3) and $\sigma_1 = 1.88$ ns, $\sigma_2 = 29.4$ ps/cm, $\sigma_3 = 90$ ps. (b) Mean time resolution of side 2. The dashed line is the fit with function (3) and $\sigma_1 = 2.32$ ns, $\sigma_2 = 28.5$ ps/cm, $\sigma_3 = 90$ ps. (c) Mean time (dots) and half-time difference (open circles) resolution. The dashed line is the result of function (4).

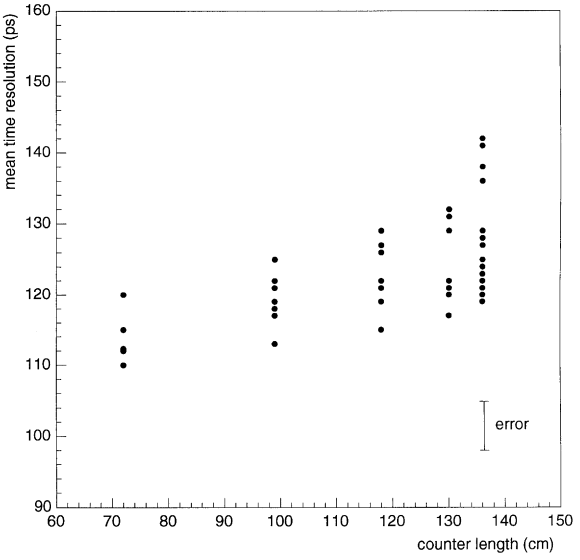

Fig. 10. The time resolution for particles hitting at the center of the counters as a function of the counter length. The magnitude of the measurement error is also shown.

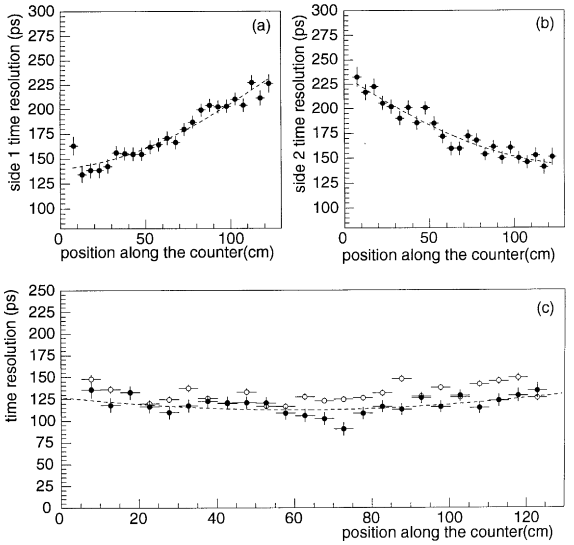

Fig. 11. Same as Fig. 9 but using the final electronics.

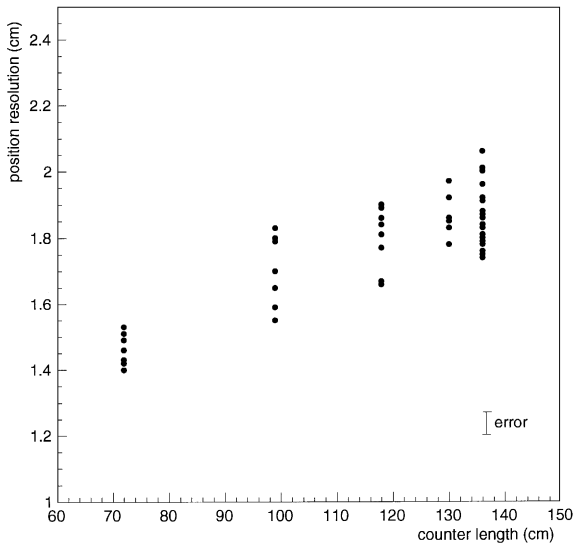

Fig. 12. Position resolution for particles hitting at the centre of the counter as a function of the counter length. The magnitude of the measurement error is also shown.

The analysis described above has been repeated using the final electronics described in Section 3.2. Fig. 11 shows the results which are very much similar to those obtained with the standard NIM/CAMAC electronics (but with a factor 50 less electric power consumption).

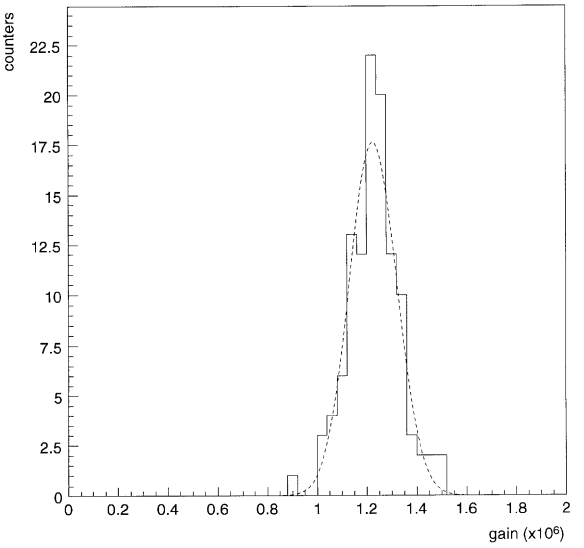

Fig. 13. Distribution of the gain for all the PMs used in the experiment.

Using formula (2), the resolution in the measurement of the impact position along the counter can be computed. Fig. 12 shows the position resolution for particles hitting at the center of the counter as a function of the counter length.

5.6. Gain measurement

LEDs positioned at the center of the counters were used to measure and monitor the gain of the PMs [9] on ground, before and after installation. Fig. 13 shows the distribution of the gain for all the PMs used in the experiment.

6. Performances in the experiment

The AMS experiment has been assembled at the end of 1997 and thoroughly tested with cosmic rays at the beginning of 1998. The preliminary results on over one million events confirm the test measurements done before the final assembly.

Fig. 14 shows the TOF between adjacent planes, corrected for the track length, for muons with momenta above 0.5 GeV and for the full apparatus acceptance. The TOF resolution is 179 ps,

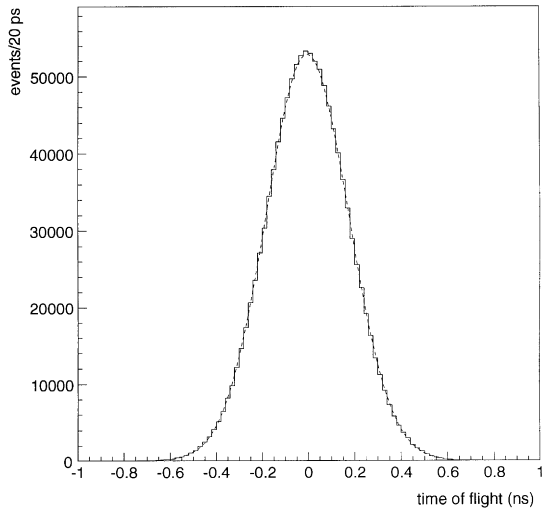

Fig. 14. The TOF between adjacent planes, corrected for the track length, for over 10^6 events taken with the AMS experiment. The dashed line is a Gaussian fit with standard deviation 179 ps.

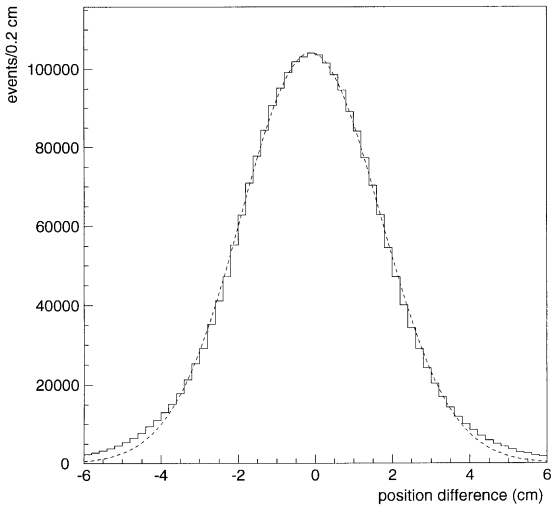

Fig. 15. The difference between the extrapolated track position and the position along the counters determined with the TOF system for over 10^6 events taken with the AMS experiment. The dashed line is a Gaussian fit with standard deviation 1.8 cm.

corresponding to a mean-time resolution of 126 ps for each plane.

Fig. 15 shows the difference between the position extrapolated by the tracker and the position along the counters determined from the time measurements (Eq.(2)). Assuming that the error on the position extrapolated by the tracker is negligible, the position resolution along the counters determined from the time measurements is 1.8 cm, corresponding to a half-time difference resolution of 113 ps.

7. Conclusions

The time-of-flight system for the AMS experiment and the associated electronics have been built according to the specifications. The main features of the system are:

- large sensitive area: 6.4 m^2;
- low-power consumption: 150 W;
- low weight: 250 kg;
- good time resolution: 120 ps;
- good position resolution: 1.8 cm;
- very compact electronics for charge and time measurement;
- space-qualified according to NASA specifications.

Acknowledgements

This work could not have been carried out without the intense and dedicated effort by the technical staff of the INFN, Bologna and of CNR-IROE, Florence. Particular thanks are due to G. Molinari and R. Pilastrini for their contribution to solving several detailed problems arising during the assembly and the integration of the system.

References

[1] AMS experiment, S.P. Ahlen et al., Nucl. Instr. and Meth. A 350 (1994) 351.
[2] D. Bollini et al., Nuovo Cimento 61A (1969) 125.
[3] A. Zichichi, Ann. Phys. 66 (1971) 405.
[4] A. Zichichi, Study of charged final states produced in e^+e^- interactions, in: Elementary Processes at High Energy, Academic Press, New York, 1971, p. 790.
[5] M. Basile et al., Nucl. Instr. and Meth. 179 (1981) 477.
[6] D. Alvisi et al., The mechanics for the TOF system of the AMS experiment, in preparation.
[7] G.K. Parks, Physics of Space Plasmas. An Introduction, Addison-Wesley, Reading, MA, 1991.
[8] D. Alvisi et al., Low power, high resolution electronics for the TOF system of the AMS experiment, in preparation.
[9] B. Bencheikh et al., Nucl. Instr. and Meth. A 315 (1992) 349.